Unifying Redox Kinetics for Standard and Fast NH_3-SCR over a V_2O_5-WO_3/TiO_2 Catalyst

Isabella Nova, Cristian Ciardelli, and Enrico Tronconi
Dipartimento di Energia, Laboratorio di Catalisi e Processi Catalitici, Politecnico di Milano, Piazza L. da Vinci 32, I-20133 Milano, Italy

Daniel Chatterjee and Michel Weibel
Daimler AG, Abteilung RBP/C, GR/VPE, D-70546 Stuttgart, Germany

DOI 10.1002/aic.11750
Published online April 28, 2009 in Wiley InterScience (www.interscience.wiley.com).

A dynamic Mars–van Krevelen kinetic model that unifies Standard and Fast SCR reactions into a single redox approach is herein proposed for V-based catalysts for NO_x removal from Diesel exhausts. Such a mechanistic model is consistent with the detailed catalytic chemistry proposed for the NH_3-NO/NO_2 reacting system in which NO_2 disproportionates to form nitrites and nitrates, nitrates are reduced by NO to nitrites in a key redox step, and nitrites react with NH_3 to form N_2 via decomposition of unstable ammonium nitrite. Intrinsic kinetic parameters were estimated by global multiresponse nonlinear regression of 42 transient runs. The model accounts for stoichiometry, selectivity, and kinetics of the global SCR process, reproducing successfully both the steady-state and transient behaviors of the SCR reacting system over the full range (0–1) of NO_2/NO_x feed ratios in the 175–425°C temperature range. © 2009 American Institute of Chemical Engineers *AIChE J,* 55: 1514–1529, 2009
Keywords: SCR DeNO$_x$, dynamic methods, standard and fast SCR kinetics, redox kinetics, Diesel exhaust aftertreatment

Introduction

The selective catalytic reduction (SCR) technology, based on the reaction between nitrogen oxides in the flue gases and NH_3/urea, has become one of the most promising technological solutions for the abatement of NO_x emissions from Diesel vehicles.[1] First commercialized in 2005 by Daimler for Euro 4 and Euro 5 compliant heavy duty applications, it is now being considered also for light duty and passenger cars to conform to the upcoming Euro 6 regulations in Europe and to the even more stringent Tier 2 Bin 5 regulations in the United States.

Although most of the research is currently focused on the study of zeolite-based catalysts,[2–13] traditional extruded SCR monoliths made of V_2O_5-WO_3/TiO_2 catalysts are still used in Europe at a commercial scale. Extensive work was devoted in the past to study V_2O_5-WO_3/TiO_2 catalysts for DeNO$_x$ing of stack gases from power plants and other stationary sources[14,15]: in such cases V-based catalysts showed the best performances in the 300–400°C *T*-range where the Standard SCR reaction was active according to the stoichiometry

$$2NH_3 + 2NO + {}^1/_2O_2 \rightarrow 2N_2 + 3H_2O \qquad (R.1)$$

However, moving from stationary to mobile applications, a wider *T*-window has to be addressed[1]: in particular, a greater activity in the low-temperature region is required. Such a need is fulfilled by positioning an onboard Diesel oxidation catalyst upstream of the SCR converter to partially convert NO to NO_2; this permits the occurrence of the Fast SCR reaction, in which an equimolar mixture of NO and NO_2 react with ammonia to form nitrogen and water:

$$2NH_3 + NO + NO_2 \rightarrow 2N_2 + 3H_2O \qquad (R.2)$$

Correspondence concerning this article should be addressed to E. Tronconi at enrico.tronconi@polimi.it

At low temperatures, in fact, the Fast SCR reaction R.2 results to be considerably faster than the Standard SCR.[3,11,16–18]

However, at the time when the first SCR-based catalytic converters were being developed at commercial scale, limited information was present in the open literature concerning the chemistry, the catalytic mechanism and the kinetics of the SCR process in the presence of both NO and NO_2, mostly related to the pioneering work of Koebel and coworkers.[16–18]

On the other hand, such information is key to the development of unsteady kinetic models of the SCR process for mobile applications: simulation tools able to describe the performance of a catalytic converter as a function of the several operating parameters has been proven to be very useful in the development and design of new technologies, but their capability in predicting accurately NO_x and ammonia emissions mainly relies on the close adherence of kinetic schemes to the real catalytic process.

Accordingly, an extensive investigation of reactivity, chemistry and catalytic mechanism of the full NH_3-NO/NO_2 SCR reacting system over V_2O_5-WO_3/TiO_2 has been recently performed in our laboratories.[19–24] Eventually, the bulk of information acquired from such an analysis were merged in a unified redox mechanism for both the Standard and the Fast SCR reactions.[25] In such a scheme, a single catalyst reduction step is considered, which involves the coparticipation of ammonia and NO. As opposite, the rate controlling reoxidation of the V catalyst sites involves gaseous oxygen, when NO_x include nitric oxide only, whereas in the presence of NO_2 as well a much higher reoxidation rate is obtained at the expense of surface nitrates formed by NO_2 adsorption onto the catalyst surface. As a result, the rate determining step of the redox process, that is, the reoxidation of V-sites, is radically changed in the Fast SCR, being carried out by nitrates, which replace gaseous oxygen. Surface nitrates are formed via disproportion of NO_2 simultaneously with nitrites, possibly onto nonreducible oxide components other than vanadium; nitrites are then oxidized to nitrates by NO_2 or preferentially decomposed to N_2 via reaction with NH_3 in the presence of ammonia. A similar reaction sequence has been recently invoked to explain the formation of ammonium nitrate observed over TiO_2 and over a Ba-Na Y-zeolite,[6] as well as the formation[26] of surface nitrates from NO_2 over Al_2O_3[27] and over Fe- and Cu-exchanged zeolites.[10,11,12,13]

On the basis of such a catalytic chemistry, we proceed in the following to derive a complete redox kinetic model for both Standard and Fast NH_3-SCR reactions over V-based catalysts. Such a model represents an extension of the model presented in Ref. 28, which was specifically obtained for the Standard SCR reaction only (i.e., no NO_2 in the system).

Experimental

For the purposes of this study new unsteady kinetic NH_3-SCR experiments of different nature were performed over the same commercial extruded V_2O_5-WO_3/TiO_2 catalyst with medium-high V-content investigated in previous work,[19–29] originally supplied by Daimler as an extruded honeycomb monolith. Experimental details have been already reported elsewhere.[19,28] Briefly, the catalyst was ground to powder (140–200 mesh), a sample (160 mg) was diluted with 80 mg of quartz and loaded in a flow-microreactor consisting of a quartz tube (6 mm i.d.) directly connected both to a UV analyzer (ABB Limas 11-HW) and to a quadrupole mass spectrometer (Balzers QMS 200), which operated in parallel.[29]

The dynamics of the NH_3 + NO + NO_2 SCR reactions were investigated using transient response methods (TRM) that consist in performing stepwise changes of concentration of one species in the feed mixture by means of fast response pulse valves,[20] which ensure constant conditions of pressure and global flow. The temperature was normally constant during each experiment, as confirmed by a thermocouple directly immersed in the catalyst bed. TRM runs were typically carried out in the presence of oxygen (2%) and water vapor (1%) in the temperature range 175–425°C, whereas the feed concentrations of NH_3, NO, and NO_2 were varied between 150 and 1000 ppm.

In particular, the effect of the NO/NO_2 feed ratio (R = NO/NO_2 = 0/1–1/0) on the SCR activity was investigated over the whole T-range. More TRM experiments were performed at 200°C with R = 1/1 to analyze the influence of the NH_3 (1000, 700, 550 ppm), NO_x (1000, 700, 550, 300 ppm), and water (0–10% v/v) feed contents, as well. In addition, the effect of oxygen (2–6% v/v) was studied by TPR experiments: all the reactants were fed at constant temperature (175°C) and afterward a temperature ramp at 10°C/min was run.

To gain kinetically relevant information, a relatively high gas hourly space velocity of 210,000 h^{-1} was used in all the experiments due to the strong $DeNO_x$ activity in the presence of NO_2.

The use of He as carrier gas allowed the evaluation of overall N-balances, which always closed within ±5% at steady-state in all the considered kinetic runs.

Intraparticle gradients and gas-solid mass transfer limitations were ruled out by theoretical diagnostic criteria,[30] as discussed in the Appendix.

Results and Discussion

Derivation of a dual site, redox rate expression for NO + NO_2 reduction with NH_3

On the basis of the results of the mechanistic investigation illustrated in previous papers,[22–25] in the following, we propose the derivation of a global kinetic model for the full NH_3-NO/NO_2 SCR reacting system, wherein, we extend the dual-site redox kinetics already presented and validated in Ref. 28 for the NH_3-NO/O_2 reacting subsystem.

In agreement with spectroscopic and mechanistic evidence,[31–34] it was proposed that S_1-sites are associated with vanadyl species, whereas S_2-sites are associated with other nonreducible, acidic surface sites, such as Vanadium-related Brønsted or Lewis sites, or also with sites related to the other oxide catalyst components.

Starting from oxidized S_1 sites (S_1 = O), the redox cycle can be written as follows:

Catalyst Reduction:

(a) $S_1 = O + NO \iff S_1 = O[NO]$

(b) $S_2 + NH_3 \leftrightarrow S_2[NH_3]$

(c) $S_1 = O[NO] + S_2[NH_3] \rightarrow N_2 + H_2O + S_1\text{-}OH + S_2$

Catalyst Reoxidation:

(d) $S_1\text{-OH} + {}^1/_4O_2 \rightarrow S_1 = O + {}^1/_2H_2O$

(e) $S_1\text{-OH} + S_2[HNO_3] \rightarrow S_1 = O + NO_2 + H_2O + S_2$

In addition, we consider also the following nonredox reaction steps:

Ammonia spillover:

(f) $S_1 + S_2[NH_3] \leftrightarrow S_1[NH_3] + S_2$

Nitrates formation:

(g) $2NO_2 + H_2O \leftrightarrow HONO + HNO_3$

(h) $HONO + S_2[NH_3] \rightarrow N_2 + 2H_2O + S_2$

(i) $HNO_3 + S_2 \leftrightarrow S_2[HNO_3]$

Step (a) accounts for a weak NO adsorption on the redox S_1 sites, whereas step (b) accounts for a strong ammonia adsorption on S_2 sites.

As evidenced in Ref. 25, the reduction of S_1 sites requires the copresence of adsorbed ammonia and NO [step (c)] for both the Standard and the Fast SCR reactions, whereas reoxidation of S_1 is performed either by gaseous oxygen [step (d)] in the case of the Standard SCR reaction or by surface nitrates [step (e)] in the Fast SCR reaction.

In line with previous results,[28] step (f), that is a spillover of ammonia from S_2 sites onto S_1 sites, is also considered: this accounts for the observed ammonia inhibition at $T < 250°C$.

Steps (g)–(i) describe the formation of surface nitrates $S_2[HNO_3]$ onto the catalyst via disproportion of NO_2, in line with literature indications for V-based and zeolite SCR catalysts.[9,12,13,17] It is postulated here that surface nitrates are formed onto nonredox S_2 sites. A basis for this assumption is the observation that NO_2 disproportion with nitrates storage, as well as the related formation of ammonium nitrate in the presence of ammonia, were observed also over a V-free WO_3/TiO_2 catalyst[15,23] and over other nonredox materials.[6,26,27]

Notice that, in the absence of NO_2, and thus of surface nitrates, we are left with steps (a)–(d)[28] only, which sum up to the stoichiometry of the Standard SCR reaction

$$NO + NH_3 + {}^1/_4O_2 \rightarrow 3/2H_2O \qquad \text{(R.1)}$$

whereas the combination of steps (a)–(c), (e), and (g)–(i) results in the Fast SCR reaction

$$2NH_3 + NO + NO_2 \rightarrow 2N_2 + 3H_2O \qquad \text{(R.2)}$$

Finally, step (i) accounts for the reversible desorption of nitrates.

It is worth mentioning that nitric acid can react with ammonia to form ammonium nitrate salt,

$$HNO_3 + NH_3 \leftrightarrow NH_4NO_3 \qquad \text{(R.3)}$$

When steps (g)–(h) are considered in conjunction with R.3, we obtain the overall stoichiometry for the formation of ammonium nitrate,

$$2NO_2 + 2NH_3 \rightarrow N_2 + H_2O + NH_4NO_3 \qquad \text{(R.4)}$$

that was indeed observed at low temperatures in several SCR runs with excess NO_2.[20,22,23]

Notice that NO_2 plays no direct role in the redox cycle. Indeed, we have shown[25] that in T-ramp experiments the rate of NO conversion at low T was essentially identical either when feeding $NO + NH_3 + NO_2$ to a clean V-catalyst, or when feeding $NO + NH_3$ only, that is, in the absence of gaseous NO_2, to the same V-catalyst presaturated with nitrates.

The overall balances of S_1- and S_2-sites yield:

$$S_1\text{-sites}: \; 1 = \sigma_{=O} + \sigma_{NO} + \sigma_{OH} + \sigma_{NH_3} \qquad (1)$$

$$S_2\text{-sites}: 1 = \theta_{free} + \theta_{NH_3} + \theta_{HNO_3} \qquad (2)$$

where the terms in the RHS of Eq. 1 represent the fractional coverages of $S_1 = O$, $S_1 = O[NO]$, S_1-OH and $S_1[NH_3]$, respectively, whereas θ_{NH_3} and θ_{HNO_3} in Eq. 2 indicate the fractional coverages of $S_2[NH_3]$ and of $S_2[HNO_3]$, respectively.

Next, we express the rates of step (c), that is, the surface reaction between activated NO and adsorbed NH_3, involving reduction of S_1-sites, and of steps (d) and (e), involving reoxidation of S_1-sites, as

$$r_{red} = r_{(c)} \; = \; k_{NO} \, C_{NO} \, \theta_{NH_3} \, \sigma_{=O} \qquad (3)$$

$$r_{reox} = r_{(d)} + r_{(e)} = (k_{ox1} \, p_{o_2}^{1/4} + k_{ox2}\theta_{HNO_3})\sigma_{OH} \qquad (4)$$

Following a Mars–van Krevelen approach, we now impose that the rate of reduction r_{red} equals r_{reox}, the overall rate of oxidation, and thus, we end up with the following relationship between the surface concentrations of reduced S_1 sites (σ_{OH}) and of oxidized S_1 sites ($\sigma_{=O}$):

$$\sigma_{OH} = \frac{k_{NO} \, C_{NO} \, \theta_{NH_3}}{k_{ox1} \, p_{O_2}^{1/4} \; + k_{ox2} \; \theta_{HNO_3}} \; \sigma_{=O} \qquad (5)$$

Notice that in so doing, we account for both V-reoxidation routes due to the action of gaseous oxygen and of surface nitrates, respectively.

On further neglecting the surface concentration of NO because of its weak adsorption, from Eq. 1 we obtain

$$1 - \sigma_{NH_3} = \left(1 + \frac{k_{NO} C_{NO} \theta_{NH_3}}{k_{ox1} p_{O_2}^{1/4} + k_{ox2} \theta_{HNO_3}}\right) \sigma_{=O} \qquad (6)$$

Under the limiting assumption of fast NH_3 spillover[28] we can invoke quasi-equilibrium for step (f) and derive

$$1 - \sigma_{NH_3} = \left(\frac{1}{1 + K_{NH_3} \frac{\theta_{NH_3}}{1 - \theta_{NH_3} - \theta_{Nit}}}\right) \qquad (7)$$

Thus, on combining Eqs. 6 and 7 with Eq. 3, we eventually obtain

$$r_{DeNOx} = r_{red} = r_{re\,ox} = \frac{k_{NO} C_{NO} \theta_{NH_3}}{\left(1 + K_{NH_3} \frac{\theta_{NH_3}}{1 - \theta_{NH_3} - \theta_{HNO_3}}\right) \cdot \left(1 + \frac{k_{NO} C_{NO} \theta_{NH_3}}{k_{ox1} p_{O_2}^{1/4} + k_{ox2} \theta_{HNO_3}}\right)} \qquad (8)$$

Notably, Eq. 8 expresses the overall reduction rate of NO, associated with both the Standard SCR reaction r_{std} [reaction (R.1)], and the Fast SCR reaction r_{fst} [reaction (R.2)]: thus $r_{DeNO_x} = r_{std} + r_{fst}$

Asymptotic analysis of the redox rate equation

It is interesting to examine the asymptotic behavior of the rate law Eq. 8 under different conditions. In the absence of NO_2, $\theta_{HNO_3} \rightarrow 0$ and Eq. 8 reduces to the dual-site modified redox rate law derived for the Standard SCR reaction in Ref. 28.

$$r_{std} = \frac{k_{NO} C_{NO} \theta_{NH_3}}{\left(1 + K_{NH_3} \frac{\theta_{NH_3}}{1-\theta_{NH_3}}\right) \cdot \left(1 + k_{O_2} \frac{C_{NO}\theta_{NH_3}}{p_{O_2}^{1/4}}\right)} \tag{9}$$

where $k_{O_2} = k_{NO}/k_{ox1}$.

Indeed, in the case of the NH_3-NO/O_2 reacting system Eq. 9 could successfully reproduce the slight promoting action of O_2 and the inhibiting action of ammonia observed in several transient runs at low temperature. It was further shown that such a model could be applied to simulate the complex dynamic behavior of real exhaust gas aftertreatment systems for vehicles,[28] resulting from the existence of an optimal ammonia surface coverage at low temperatures.

Also, it was shown that Eq. 9 can be further simplified in the case of low-ammonia coverages, as prevailing, for example, at temperatures above 250–300°C. Under these conditions, we recover the well known Eley–Rideal form

$$r_{std} = k_{NO} \cdot C_{NO} \cdot \theta_{NH_3} \tag{10}$$

Equation 10 is extensively used in the kinetic literature for SCR stationary applications,[15,35,36] which indeed operate typically at T higher than 250°C.

Notice that in Eq. 8 k_{NO}, K_{NH_3}, and k_{ox1} ($k_{O1} = k_{NO}/k_{ox2}$)-are parameters related to the occurrence of the Standard SCR reaction only: indeed, they are the same as in Eq. 9, thus, the parameter estimates obtained from the fit of experiments run in the absence of NO_2[28] can still be used.

Just one more parameter is added in Eq. 8, that is k_{ox2} or, in a reparameterized form, $D = k_{ox2}/k_{ox1}$: this, reflecting the ratio of the rate of reoxidation step by nitrates over that performed by oxygen, is expected to be much higher than 1 in the presence of NO_2 in the feed.

To decouple the contributions of r_{std} and r_{fst} in the overall NO reduction rate r_{deNOx}, we consider that

$$r_{DeNOx} = r_{std} + r_{fst} = r_{(e)} + r_{(d)}, \tag{11}$$

and that

$$\frac{r_{(e)}}{r_{(d)}} = D \frac{\theta_{HNO_3}}{p_{O_2}^{1/4}} \tag{12}$$

Accordingly,

$$r_{std} = r_{DeNOx} \frac{1}{1 + D \frac{\theta_{HNO_3}}{p_{O_2}^{1/4}}} \tag{13}$$

and r_{fst} can be obtained from $r_{DeNOx} - r_{std}$.

Finally, it is worth noticing that according to Eq. 8, the Fast SCR should be active even in the absence of oxygen, the reoxidation of the V-sites being carried out by nitrates only: in such a case, the $deNO_x$ rate expression Eq. 8 reduces in fact to

$$r_{NO} = \frac{k_{NO} C_{NO} \theta_{NH_3}}{\left(1 + K_{NH_3} \frac{\theta_{NH_3}}{1-\theta_{NH_3}-\theta_{HNO_3}}\right)\left(k_{nit} \frac{C_{NO}\theta_{NH_3}}{\theta_{HNO_3}}\right)} \tag{14}$$

where $k_{nit} = k_{NO}/k_{ox2}$.

The occurrence of the Fast SCR reaction when feeding NO, NO_2, and NH_3 in the absence of gaseous oxygen was indeed observed.[25]

Rate of nitrates formation

To close the redox cycle, a kinetic expression for the rate of nitrates formation r_{amm} has to be provided. This is done assuming that step (g) is a fast unfavorably equilibrated disproportionation of NO_2, followed by the rate determining reaction of nitrous acid with adsorbed ammonia to form unstable ammonium nitrite, which readily decomposes to nitrogen [step (h)]. Accordingly,

$$r_{amm} = r_{(h)} = k_2 [HONO] \theta_{NH_3} \tag{15}$$

Assuming equilibrium for steps (g) and (i), and taking into account the balance of S_2-sites, (Eq. 2), we obtain

$$[HONO] \cong K_1 \frac{C_{NO_2}^2 (1 - \theta_{NH_3} - \theta_{HNO_3})}{\theta_{HNO_3}} \tag{16}$$

In deriving Eq. 16, we have incorporated the H_2O dependence into K_1, and assumed a small surface concentration of adsorbed nitrite species in view of their rapid reaction with ammonia.

Finally, on combining Eq. 15 with Eq. 16, and setting $k_{amm} = (K_1\, k_2)$, we get

$$r_{amm} = \frac{k_{amm} C_{NO_2}^2 \theta_{NH_3} (1 - \theta_{NH_3} - \theta_{HNO_3})}{\theta_{HNO_3}} \tag{17}$$

Notice that the derivation of Eq. 17 does not involve any interaction with the redox sites S_1: as already discussed, this is indeed consistent with experimental evidence showing that formation of nitrates occurs on V-free catalysts as well on V-based systems, and with other literature indications that show nitrates formation over zeolites[6,26] and alumina-based catalysts[27] in the absence of redox components.

In line with the facile formation of nitrates already at low temperatures,[13] and with the modest T-dependence of NH_4NO_3 formation,[21,23,12] no activation energy was assigned to k_{amm}.

Complete kinetic scheme

To describe the full NH_3-NO/NO_2-O_2 reacting system in the whole range of temperatures and NO_2/NO_X feed ratios, other reactions apart from those that describe the redox cycles [steps (a)–(h)], resulting in the Standard and Fast SCR reactions RS.4 and RS.5, had to be incorporated in the

Table 1. List of Reactions Included in the SCR Kinetic Model

RS.1	$S_2 + NH_3 \rightarrow S_2[NH_3]$	NH_3 adsorption	r_{ads}
RS.2	$S_2[NH_3] \rightarrow S_2 + NH_3$	NH_3 desorption	r_{des}
RS.3	$S_2[NH_3] + {}^3/_4O_2 \rightarrow {}^1/_2N_2 + {}^3/_2H_2O$	NH_3 oxidation	r_{ox}
RS.4	$NO + S_2[NH_3] + {}^1/_4O_2 \rightarrow N_2 + {}^3/_2H_2O + S_2$	Standard SCR	r_{NO}
RS.5	$NO + S_2[HNO_3] + S_2[NH_3] \rightarrow N_2 + 2H_2O + NO_2 + 2S_2$	Fast SCR	r_{fst}
RS.6	$2NO_2 + S_2[NH_3] \rightarrow N_2 + H_2O + S_2[HNO_3]$	Nitrates formation	r_{amm}
RS.7	$HNO_3 + S_2 \rightarrow S_2[HNO_3]$	Nitrates adsorption	r_{adnit}
RS.8	$S_2[HNO_3] \rightarrow HNO_3 + S_2$	Nitrates desorption	r_{desnit}
RS.9	$S_2[NH_3] + {}^3/_4NO_2 \rightarrow {}^7/_8N_2 + {}^3/_2H_2O$	NO_2 SCR	r_{NO_2}
RS.10	$S_2[NH_3] + S_2[HNO_3] \rightarrow N_2O + 2H_2O + S_2$	N_2O formation	r_{N_2O}

kinetic model.[20,21] Such additional reaction steps include ammonia oxidation (RS.3), nitrates adsorption and desorption (RS.7-8), NO_2 SCR (RS.9), and N_2O formation (RS.10).

The set of global reactions taken into account in the kinetic model is listed in Table 1. The corresponding adopted rate equations are discussed in the following.

In line with previous findings[19,38] Temkin-type NH_3 adsorption/desorption kinetics, with a nonactivated adsorption step, were assumed for reactions (RS.1)–(RS.2),

$$r_{ads} = k_{ads} C_{NH3}(1 - \theta_{NH_3} - \theta_{HNO_3}) \tag{18}$$

$$r_{des} = k^{o}_{des} \exp[-\frac{E^{\circ}_{des}}{RT}(1 - \alpha\theta_{NH_3})]\theta_{NH_3} \tag{19}$$

The rate of ammonia oxidation, reaction (RS.3), was represented by

$$r_{ox} = k_{ox}\theta_{NH_3} \cdot \left(\frac{p_{O_2}}{0.02}\right)^{\beta} \tag{20}$$

In line with the derivation in the previous paragraph, the dual site redox rate Eq. 8 was implemented to represent the sum of the rates of reactions RS.4 and RS.5, which involve NO reduction. Likewise, Eq. 17 was associated with the rate of nitrates formation, reaction (RS.6).

The rates of adsorption–desorption of nitrates (RS.7-8) were given the following expressions:

$$r_{adsnit} = k_{adsnit} C_{HNO_3}(1 - \theta_{NH_3} - \theta_{HNO_3}) \tag{21}$$

$$r_{desnit} = k_{desnit}\theta_{HNO_3} \tag{22}$$

The T-dependence of k_{adsnit} and k_{desnit}, which play a minor role under typical reaction conditions, was neglected to minimize the number of fitting parameters.

Finally, for the rate of the NO_2 SCR reaction (RS.9) and of N_2O formation (RS.10) we adopted,[37] respectively,

$$r_{NO_2S} = k^{o}_{NO2S} \exp\left(-E_{NO_2S}\Big/RT\right) C_{NO_2}\theta_{NH_3} \tag{23}$$

$$r_{N_2O} = k^{o}_{N_2O} \exp\left(-E_{N_2O}\Big/RT\right)\theta_{HNO_3}\theta_{NH_3} \tag{24}$$

Test reactor model

As in previous work, the kinetic analysis of the large set of transient data collected over the powdered V-based SCR catalyst has been addressed according to a dynamic one-dimensional isothermal heterogeneous plug-flow model of the test micro reactor[19] coupled with a nonlinear regression code.

The test reactor model comprises the following transient mass balance equations of adsorbed ammonia and nitrates, and of gaseous NH_3, N_2, NO, NO_2, N_2O, HNO_3 as reported in the following:

Adsorbed phase: NH_3 and HNO_3

$$\Omega\frac{\partial\theta_{NH_3}}{\partial t} = r_{ads} - r_{des} - r_{ox} - r_{DeNOx} - r_{amm} - r_{NO_2} - r_{N_2O} \tag{25}$$

$$\Omega\frac{\partial\theta_{HNO_3}}{\partial t} = r_{amm} + r_{adnit} - r_{desnit} - r_{fst} - r_{N_2O} \tag{26}$$

Gas phase: NH_3, N_2, NO, NO_2, N_2O, HNO_3

$$\varepsilon\frac{\partial C_{NH_3}}{\partial t} = -v\frac{\partial C_{NH_3}}{\partial z} + (1-\varepsilon)(-r_{ads} + r_{des}) \tag{27}$$

$$\varepsilon\frac{\partial C_{N_2}}{\partial t} = -v\frac{\partial C_{N_2}}{\partial z} + (1-\varepsilon)(1/2r_{ox} + r_{DeNOx} + r_{amm} + 7/8r_{NO_2}) \tag{28}$$

$$\varepsilon\frac{\partial C_{NO}}{\partial t} = -v\frac{\partial C_{NO}}{\partial z} + (1-\varepsilon)(-r_{DeNOx}) \tag{29}$$

$$\varepsilon\frac{\partial C_{NO_2}}{\partial t} = -v\frac{\partial C_{NO_2}}{\partial z} + (1-\varepsilon)(r_{fst} - 2r_{amm} - 3/4r_{NO_2}) \tag{30}$$

$$\varepsilon\frac{\partial C_{N_2O}}{\partial t} = -v\frac{\partial C_{N_2O}}{\partial z} + (1-\varepsilon)r_{N_2O} \tag{31}$$

$$\varepsilon\frac{\partial C_{HNO_3}}{\partial t} = -v\frac{\partial C_{HNO_3}}{\partial z} + (1-\varepsilon)(-r_{adnit} + r_{desnit}) \tag{32}$$

In line with previous findings,[21–23] we further assume that any gaseous HNO_3 leaving the test reactor would react with NH_3 according to R.3 to form NH_4NO_3, which would therefore go undetected and build-up somewhere downstream from the reactor, thus giving rise to a lack in the overall N-balance.

The set of PDEs (25–32), with obvious initial and boundary conditions, was solved numerically according to the

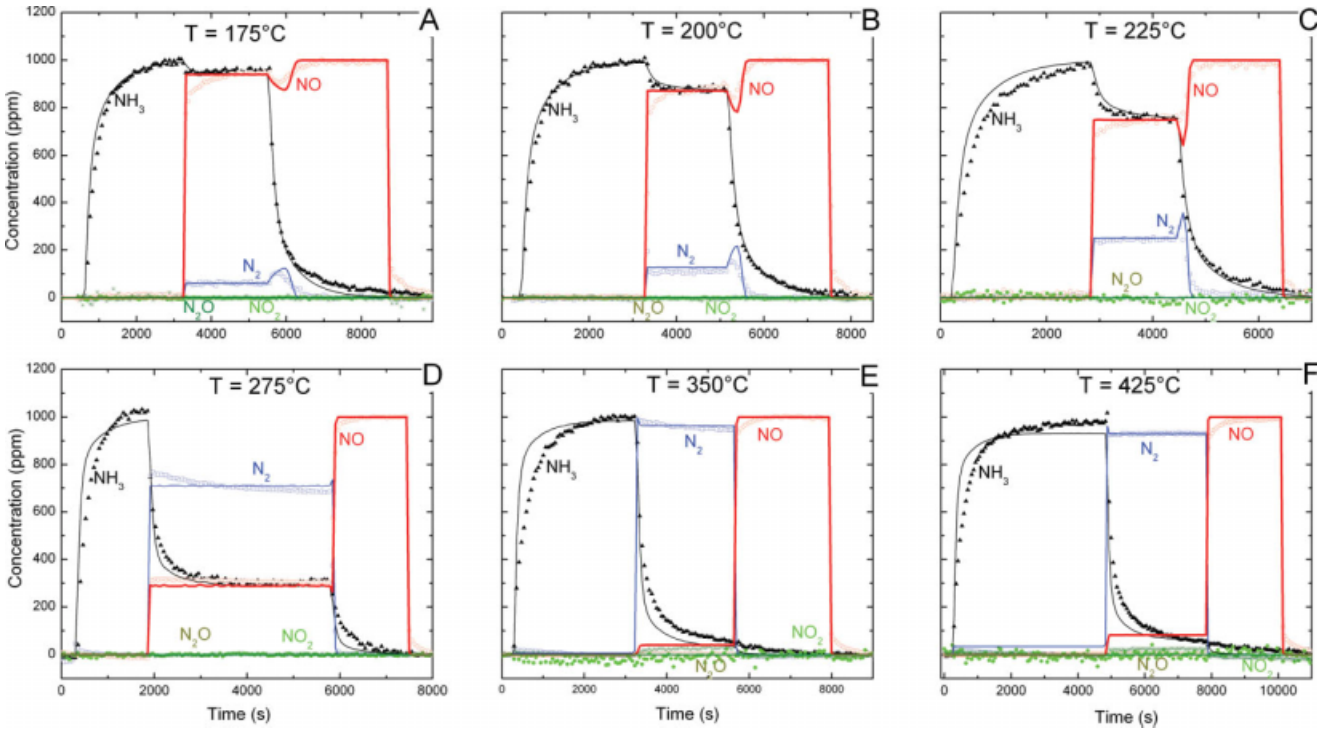

Figure 1. Transient SCR microreactor experiments with step feed of NH_3 (0, 1000, 0 ppm) in NO (1000 ppm) + O_2 (2% *v/v*) and H_2O (1% *v/v*) + He at 175 (A), 200 (B), 225 (C), 275 (D), 350 (E), and 425°C (F).

Symbols: measured concentrations of NH_3, NO, N_2, NO_2, and N_2O at reactor outlet. Lines: kinetic fit. [Color figure can be viewed in the online issue, which is available at www.interscience.wiley.com.]

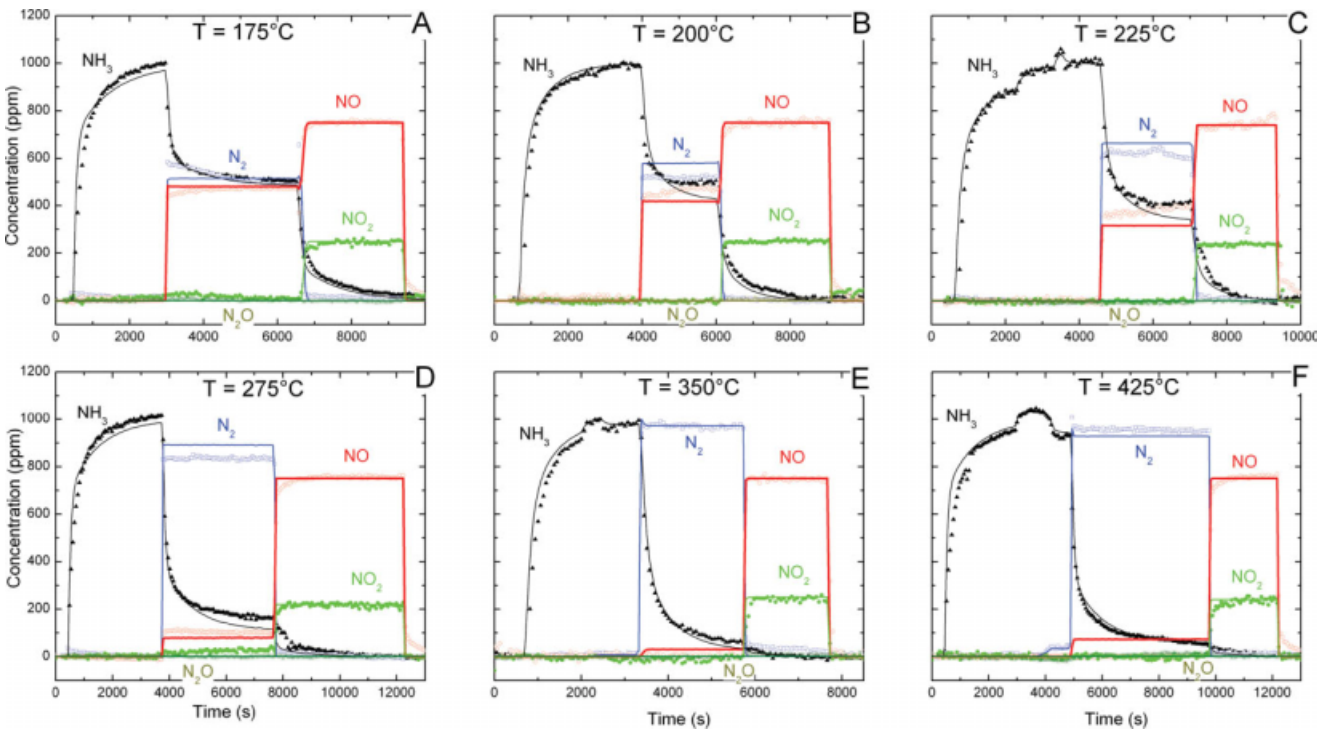

Figure 2. Transient SCR microreactor experiments with step feed of NH_3 (0, 1000, 0 ppm) in NO (750 ppm) +NO_2 (250 ppm) + O_2 (2% *v/v*) and H_2O (1% *v/v*) + He at 175 (A), 200 (B), 225 (C), 275 (D), 350 (E), and 425°C (F).

Symbols: measured concentrations of NH_3, NO, N_2, NO_2, and N_2O at reactor outlet. Lines: kinetic fit. [Color figure can be viewed in the online issue, which is available at www.interscience.wiley.com.]

method of lines, based on axial discretization with backward finite differences and on time integration by Gear's algorithm.

An empirical model of the ammonia response function of the rig and of the analyzers was adopted to describe the delayed NH_3 evolution[28]; the parameters were fitted to blank ammonia step change experiments (not shown).

Runs performed in previous work[19,28,39] by feeding only NH_3 in the presence of O_2 and water were used to estimate the kinetic parameters for ammonia adsorption–desorption, in Eqs. 18 and 19, and for ammonia oxidation, in Eq. 20. Also, an independent estimate of the NH_3 adsorption capacity Ω was obtained from NH_3 adsorption isotherms at low temperature.[39] The same estimates as reported in Ref. 39 have been retained in this work with no further adjustment.

The nitrates adsorption capacity was set to the same value Ω, based on adsorption runs of NO_2 showing a comparable storage of ammonia and NO_2 and in line with the assumption that ammonia and nitrates are adsorbed on the same S_2 sites.

Concerning the rate parameters in the remaining rate expressions for the SCR reactions, the temporal evolutions of the outlet NH_3, NO, N_2, NO_2, N_2O concentrations were used as fitted responses in a global multiresponse nonlinear regression of 42 different TRM experiments performed with feeds including water and oxygen, using a robust multimethod regression routine.[40,41] To minimize correlations within the numerous fitting parameters a sequential fitting strategy was followed, as described below.

Kinetic runs: effect of $R = NO/NO_2$ *feed ratio*

A systematic kinetic investigation the NH_3-NO/NO_2 SCR system was carried out over the full range of NO/NO_X feed ratios (from zero to unity) and over a representative range of temperatures (160–425°C). In total, 31 such TRM runs were performed.

Figure 1 illustrates the results obtained at different temperatures in transient reaction experiments with a $NO/NO_2 = 1/0$ feed ratio, corresponding to a feed mixture of 1000 ppm of NH_3, 1000 ppm of NO, 2% O_2 and 1% H_2O *v/v*, with balance He. As mentioned before, the same experiments were used in a previous work[28] to describe the Standard SCR reaction only and are reported here for completeness.

Considering the experiment run at 275°C (Figure 1D) ammonia was initially fed to the reactor, then, at $t = 1900$ s, NO was stepwise added to the feed. At this stage the NH_3 concentration decreased from its inlet level to about 300 ppm as it reacted with NO, at the same time the N_2 trace increased from 0 up to about 700 ppm, whereas the NO outlet concentration trace grew up to 300 ppm. The steady-state values of NH_3, NO, and N_2 were consistent with the stoichiometry of the Standard SCR reaction (R.1) with a conversion roughly of 70%. At $t = 5800$ s, the NH_3 feed was shut down, hence its outlet concentration trace quickly dropped. The N_2 signal also decreased rapidly as no reaction occurred anymore, while the NO concentration grew, eventually approaching its feed level.

As clearly apparent from the figure, and already discussed in a previous article,[28] the experiments performed above 250°C show similar dynamic features, the only effect of

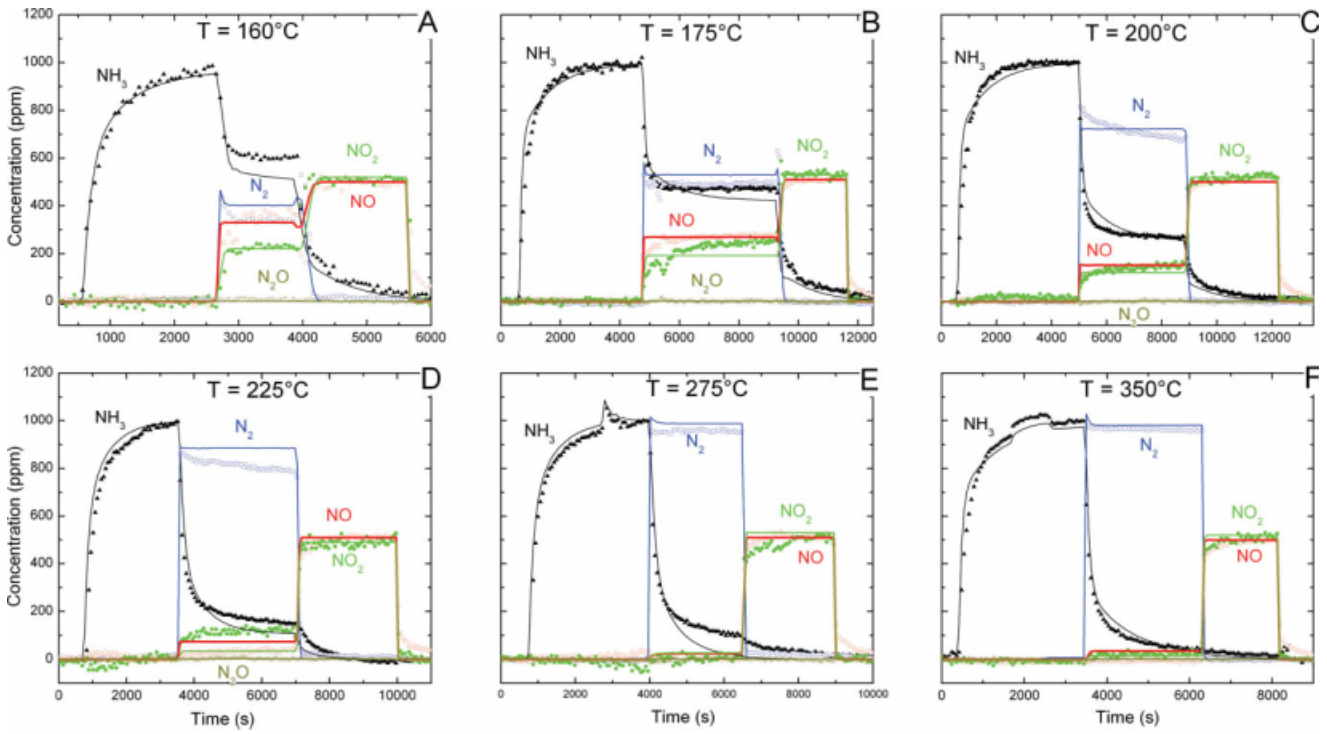

Figure 3. Transient SCR microreactor experiments with step feed of NH_3 (0, 1000, 0 ppm) in NO (500 ppm) + NO_2 (500 ppm) + O_2 (2% *v/v*) and H_2O (1% *v/v*) + He at 160 (A), 175 (B), 200 (C), 225 (D), 275 (E), and 350°C (F).

Symbols: measured concentrations of NH_3, NO, N_2, NO_2, and N_2O at reactor outlet. Lines: kinetic fit. [Color figure can be viewed in the online issue, which is available at www.interscience.wiley.com.]

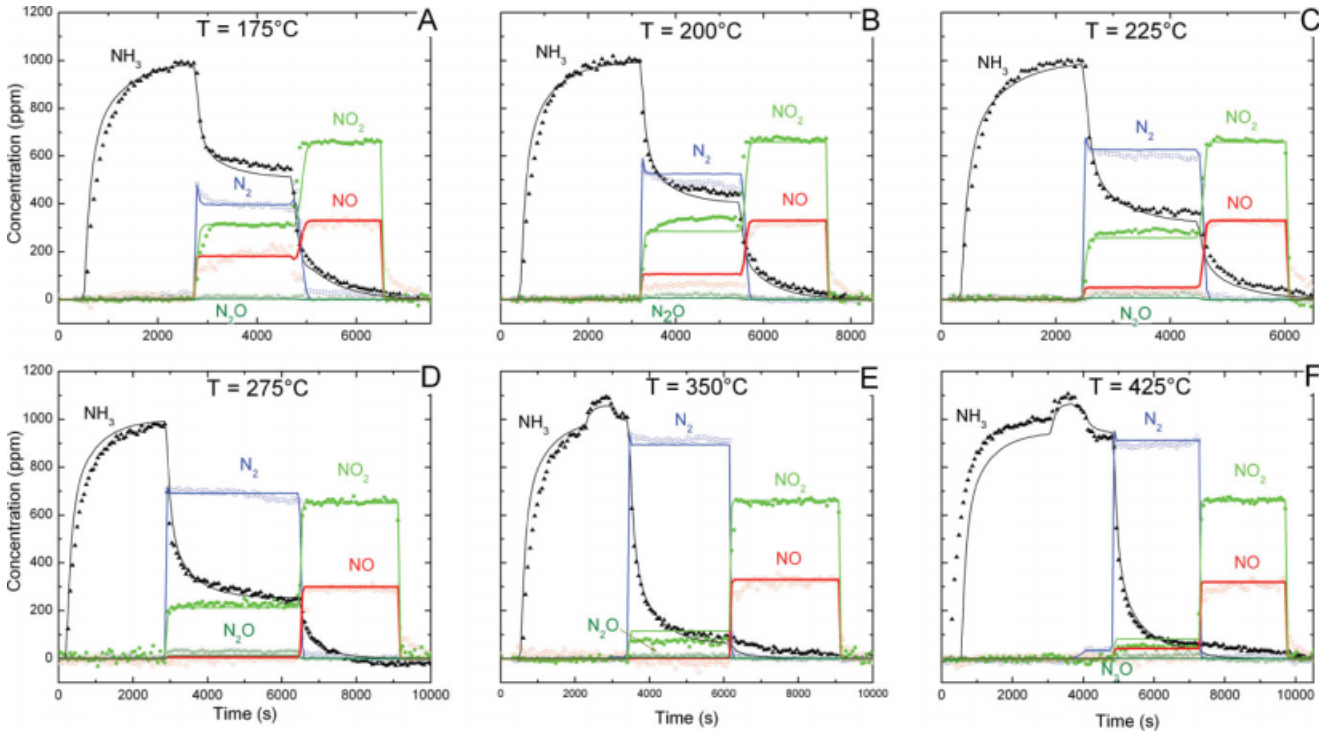

Figure 4. Transient SCR microreactor experiments with step feed of NH_3 (0, 1000, 0 ppm) in NO (330 ppm) + NO_2 (660 ppm) + O_2 (2% *v/v*) and H_2O (1% *v/v*) + He at 175 (A), 200 (B), 225 (C), 275 (D), 350 (E), and 425°C (F).

Symbols: measured concentrations of NH_3, NO, N_2, NO_2, and N_2O at reactor outlet. Lines: kinetic fit. [Color figure can be viewed in the online issue, which is available at www.interscience.wiley.com.]

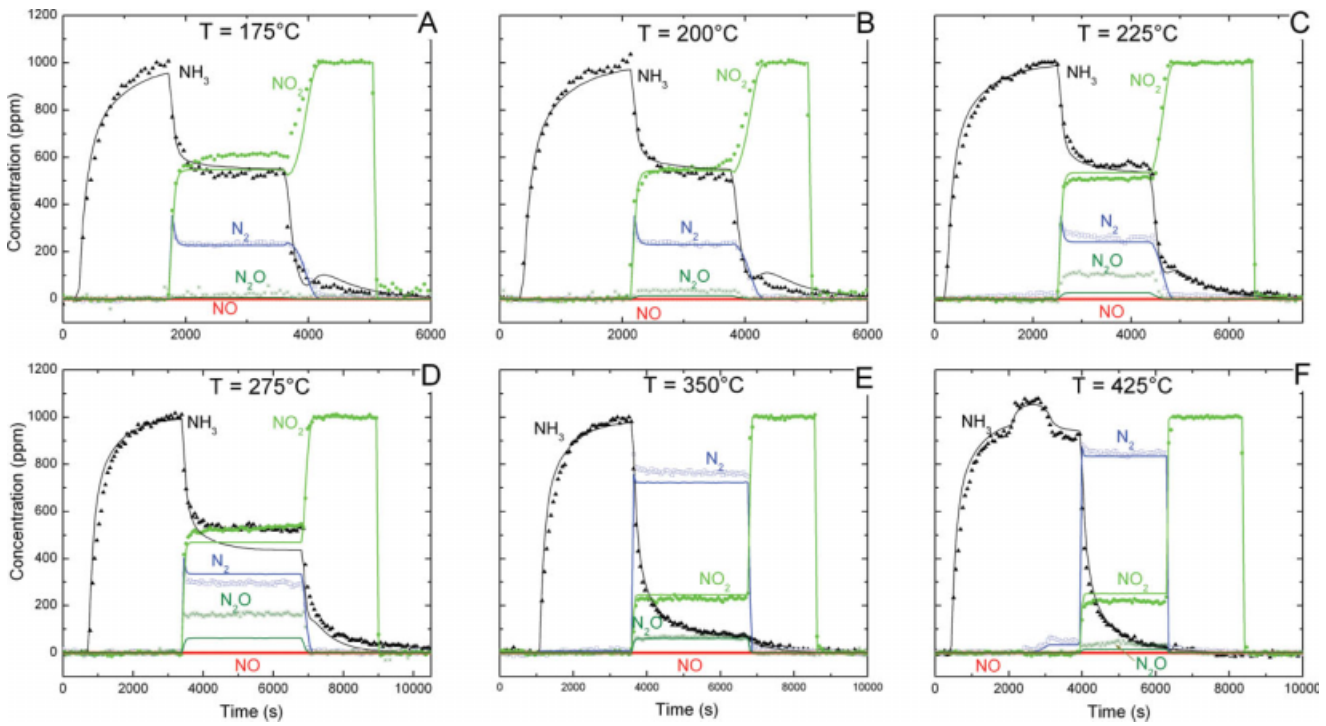

Figure 5. Transient SCR microreactor experiments with step feed of NH_3 (0, 1000, 0 ppm) in NO_2 (1000 ppm) + O_2 (2% *v/v*) and H_2O (1% *v/v*) + He at 175 (A), 200 (B), 225 (C), 275 (D), 350 (E), and 425°C (F).

Symbols: measured concentrations of NH_3, NO, N_2, NO_2, and N_2O at reactor outlet. Lines: kinetic fit. [Color figure can be viewed in the online issue, which is available at www.interscience.wiley.com.]

temperature being an increase in the NO and ammonia conversions.

Conversely, experiments performed at temperatures below 250°C (see Figure 1B, $T = 200$°C) exhibited a different dynamic behavior of NO and N_2 during both the NH_3 start-up phase and the NH_3 shut-off transient. Indeed, when ammonia was removed from the feed flow ($t = 1500$ s) the NO outlet concentration first decreased, passed through a minimum and then began to increase due to the depletion of adsorbed ammonia. A symmetrical evolution was observed for N_2, indicating that the $deNO_x$ activity of the system was temporarily enhanced until complete depletion of the residual NH_3 on the catalyst surface. This behavior was attributed to an ammonia inhibition, for example due to electronic interaction or possibly via direct blocking of the redox sites. The low-T inhibition of ammonia has been discussed in Ref. 28, where also references to the relevant literature are provided.

Figure 2 shows data collected when a stream consisting of 1000 ppm of NH_3, 750 ppm of NO, 250 ppm of NO_2, 2% O_2, and 1% H_2O, with balance He was fed to the reactor at different temperatures ($R = NO/NO_2 = 3/1$).

In the case of the experiment performed at 175°C (Figure 2A), at $t = 3000$ s the NO_x mixture was added to the ammonia feed, and the reaction took place. At steady state production of 500 ppm of nitrogen was observed, associated with total consumption of NO_2 and with consumptions of 250 ppm of NO and 500 ppm of NH_3. These values reflect exactly the stoichiometry of the Fast SCR reaction (R.2), which is undoubtedly responsible for such an enhanced activity at low T when compared with Figure 1. Indeed, the addition of NO_2 to the reacting system resulted in a marked increase of the NO_x conversion, which passed from 5% measured in the case of the Standard SCR reaction (Figure 1A), up to roughly 50%. It should be also noticed that in this run the overall $deNO_x$ efficiency was limited by the NO_2 feed concentration. In fact, analyzing the run performed at 200°C (Figure 2B), it appears that the NO_x conversion did not grow further: this is related to the fact that the limiting reactant NO_2 was totally converted already at 175°C.

At $T > 200$°C (Figure 2C/F) as expected, the Standard SCR also became significantly active, as demonstrated by the increased NH_3 and NO conversions and N_2 production. Again, the limited amount of 25% of NO_2 in the feed stream remarkably promoted the low-temperature $deNO_x$ efficiency with respect to the case in which only NO was present: in fact, at 275°C the gain in NO_x conversion was still significant (from 70 to nearly 90%).

Experiments were then performed feeding 1000 ppm of ammonia and NO and NO_2 in equimolar amounts (500 ppm each, $R = NO/NO_2 = 1/1$) in the presence of 2% O_2 and 1% H_2O, with balance He. The results in the T-range 160–350°C are reported in Figures 3A–F.

At 200°C (Figure 3C), after achieving steady state, a production of 700 ppm of nitrogen was observed, together with a consumption of 350 ppm of NO, 350 ppm of NO_2, and 700 ppm of NH_3. Such values reflect exactly the stoichiometry of the Fast SCR, reaction (R.2), with a 70% conversion of NO_x.

The Fast SCR was the prevailing reaction in the whole analyzed T-range, between 175 and 425°C, and indeed, the conversions of NO and NO_2 resulted very similar whereas the trends of ammonia and nitrogen were mirror-like, in agreement with (R.2).

Conversely, the run performed at 225°C showed a higher NO conversion with respect to NO_2: the result was explained considering the simultaneous occurrence of the Standard SCR reaction (R.1), which indeed was found to be active at such T (see Figure 1). As shown in the following (see Figure 5), at higher temperatures the NO_2 SCR reaction (RS.9) also became active on V-based systems,[16] so that the excess NO_2 detected at 225°C was consumed and total conversions of both NO and NO_2 were achieved.

A peculiar behavior was observed in the run at 160°C: a significant deviation between NO and NO_2 conversions was evident associated with a lack in the N-balance: as discussed latter, at such a low temperature NO_2 can be consumed in fact not only by the Fast SCR, but also by the ammonium nitrate formation reaction (R.4).[21–23]

Figure 4A/F shows the results of six TRM runs performed feeding 1000 ppm of NH_3, 670 ppm of NO_2, 330 ppm of NO,

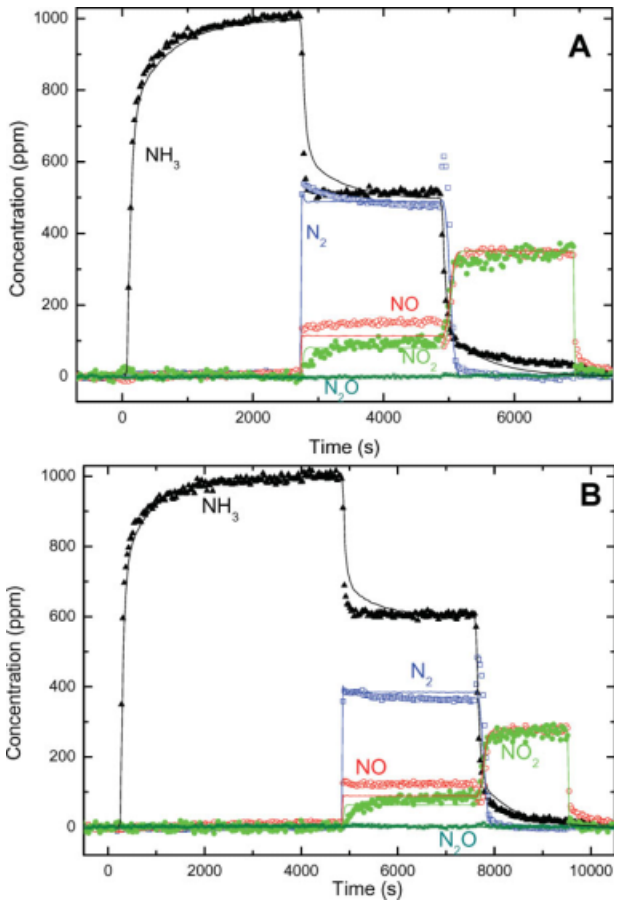

Figure 6. Transient SCR microreactor experiments with step feed of NO_x ($NO/NO_2 = 1/1$) in NH_3 (1000 ppm) + O_2 (2% *v/v*) and H_2O (1% *v/v*) + He at 200°C.

A: $NO_x = 700$ ppm and B: $NO_x = 550$ ppm. Symbols: measured concentrations of NH_3, NO, N_2, NO_2, and N_2O at reactor outlet. Lines: kinetic fit. [Color figure can be viewed in the online issue, which is available at www.interscience.wiley.com.]

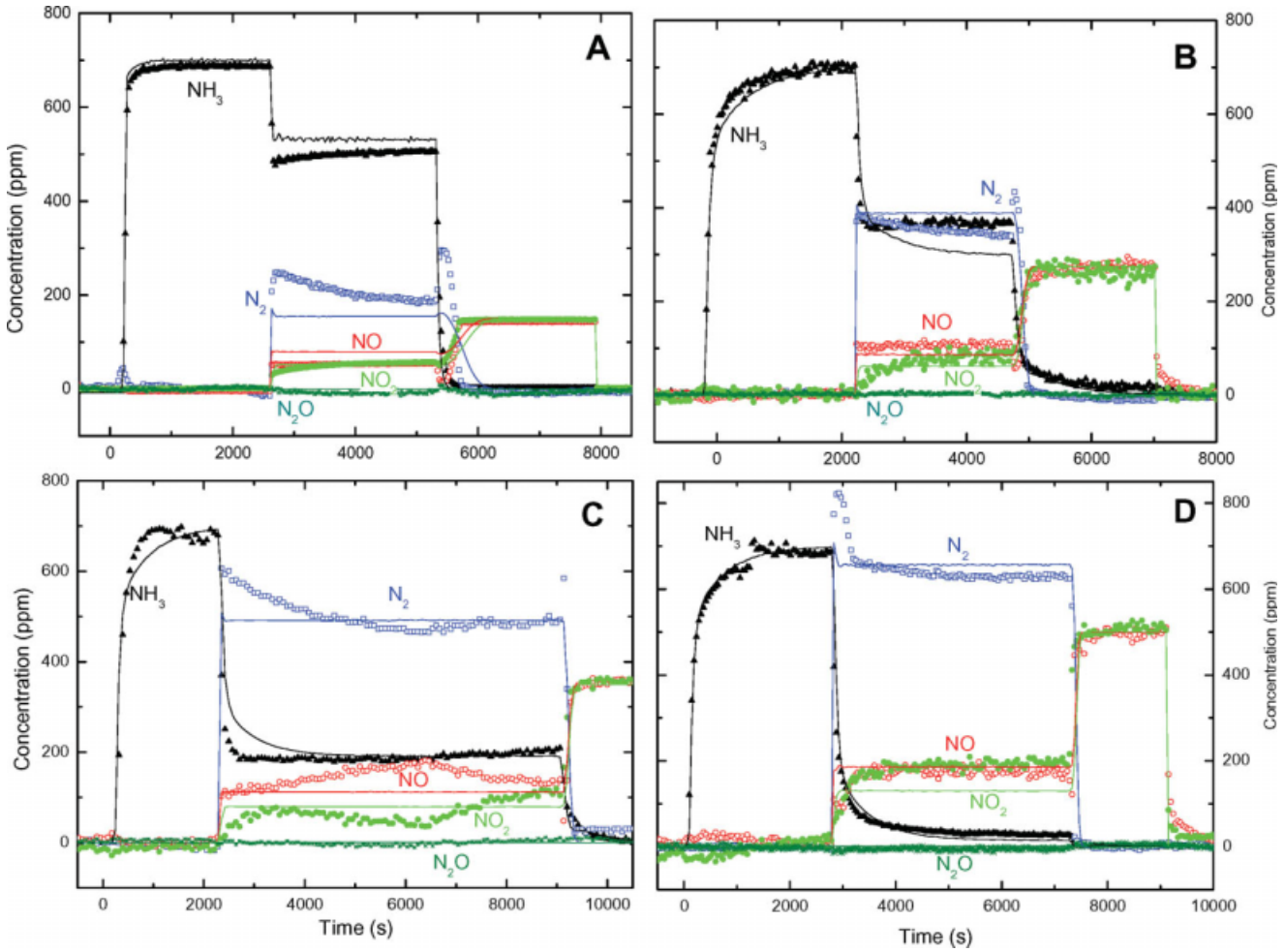

Figure 7. Transient SCR microreactor experiments with step feed of NO_x (NO/NO_2 = 1/1) in NH_3 (700 ppm) + O_2 (2% *v/v*) and H_2O (1% *v/v*) + He at 200°C.

A: NO_x = 300 ppm, B: NO_x = 550 ppm, C: NO_x = 700 ppm, and D: NO_x = 1000 ppm. Symbols: measured concentrations of NH_3, NO, N_2, NO_2, and N_2O at reactor outlet. Lines: kinetic fit. [Color figure can be viewed in the online issue, which is available at www.interscience.wiley.com.]

2% O_2, and 1% H_2O, with balance He ($R = NO/NO_2 = 1/2$), thus in excess of NO_2 in the NO_x feed mixture.

Inspection of Figure 4A/D, data obtained at $T \leq 275$°C, indicates that all the NO in the feed was consumed according to the Fast SCR stoichiometry, reaction (R.2), whereas the steady state concentrations of the other species points out also the formation of ammonium nitrate (R.4) and of N_2O (RS.10). At higher temperatures (Figure 4E/F), an enhanced consumption of reactants was observed, accompanied by production of nitrogen. This feature is ascribed to the onset of the NO_2-SCR reaction (RS.9).

To investigate the reactivity of the SCR system in the presence of NH_3 + NO_2 only, TRM runs were performed in the 175–425°C range using a feed mixture containing 1000 ppm of NH_3, 1000 ppm of NO_2, 2% O_2, and 1% H_2O, with balance He: the results are reported in Figure 5A/F.

At T = 175°C (Figure 5A), as soon as NO_2 was fed to the reactor an equimolar consumption of the two reactants NO_2 and NH_3 with a simultaneous production of nitrogen was observed. As documented in previous articles, this situation is well explained by the occurrence of reaction (R.4), with a conversion of about 50%[16,17,21–23]: this reaction involves in fact formation of solid ammonium nitrate, a salt that is in equilibrium with gaseous HNO_3 and NH_3 below about 170°C. Indeed, in this experiment a lack of 25% in the N-balance at steady-state was apparent,[20] which is ascribed to the precipitation of a corresponding amount of NH_4NO_3 and is consistent with the concentrations of ammonia, NO_2, nitrogen, and NH_4NO_3 according to the stoichiometry of reaction (R.4).

By increasing the temperature of the experiments (Figure 5B/F), N_2O appeared among the reaction products, possibly due to a partial decomposition of ammonium nitrate species (reaction RS.10) and its concentration increased up to 275°C. In the high-temperature region (Figure 5D/F), a sudden increase in the conversion of the reactants NO_2 and NH_3 and in the production of nitrogen was observed. This was due to the onset of the NO_2 SCR, reaction (RS.9), which involves conversion of NH_3 and NO_2 in nonequimolar amounts.

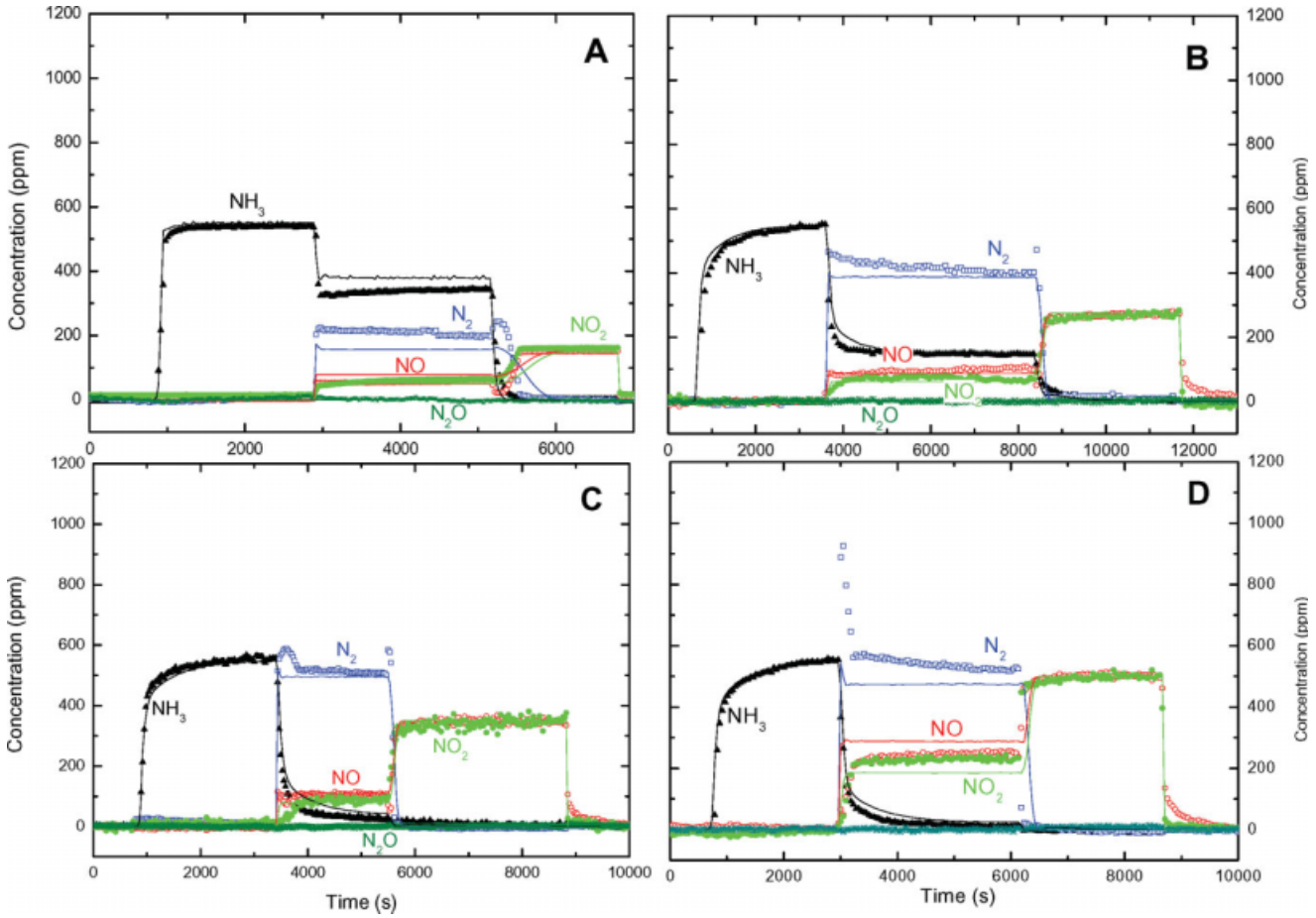

Figure 8. Transient SCR microreactor experiments with step feed of NO_x (NO/NO_2 = 1/1) in NH_3 (550 ppm) + O_2 (2% *v/v*) and H_2O (1% *v/v*) + He at 200°C.

A: NO_x = 300 ppm, B: NO_x = 550 ppm, C: NO_x = 700 ppm, and D: NO_x = 1000 ppm. Symbols: measured concentrations of NH_3, NO, N_2, NO_2, and N_2O at reactor outlet. Lines: kinetic fit. [Color figure can be viewed in the online issue, which is available at www.interscience.wiley.com.]

Kinetic runs: effects of NO_x and ammonia feed concentrations

The influence of the reactants feed concentrations on the activity of the Fast SCR reaction (R.2) was investigated by means of 11 additional TRM runs, where a feed containing NO_x with constant $R = NO/NO_2 = 1$ was stepwise added to a feed stream of NH_3, O_2 (2%), H_2O (1%) and balance helium at 200°C. The runs included different ammonia (1000, 700, and 550 ppm) and NO_x (1000, 700, 550, and 300 ppm) feed contents.

The data collected varying the NO_x feed concentrations for constant ammonia feed are reported in Figure 6A/B (1000 ppm of ammonia), Figure 7A/D (700 ppm of ammonia), and Figure 8A/D (550 ppm of ammonia), in terms of outlet concentration profiles of ammonia, NO, NO_2, N_2, and N_2O (symbols).

In any case, the steady state levels of reactants and products agreed as expected with the stoichiometry of the Fast SCR reaction (R.2), with an overall conversion which was only slightly affected by the variation of the reactant concentrations.

Minor differences were found only in the dynamics of reactants admission or removal from the reactor: indeed, by increasing the NO_x concentration or by decreasing that of ammonia, an enhancement of the transient features associated with NO_x admission was evident; conversely, the transient behaviors at NH_3 shutoff seemed more marked when decreasing NO_x concentration or increasing ammonia content. This effect can still be related to the ammonia inhibition effect already discussed.

The comparison of the steady state reactivity values of the experiments that were not limited by the total consumption

Table 2. Orders of Magnitude of the Rate Parameter Estimates for Reactions RS.5 and RS.10

Reaction	Rate Parameters	Estimates
RS.5	$D = k_{ox1}/k_{ox2}$ ($bar^{1/4}$)	4.3×10^3
RS.6	k_{amm} (m^3/mol/s)	1.3×10^3
RS.7	k_{adnit} (1/s)	4.0
RS.8	k_{desnit} (mol/m^3/s)	1.3×10^1
RS.9	k^o_{NO2S} (1/s)	3.4×10^{12}
	E_{NO_2S} (kJ/mol)	110
RS.10	k^o_{NO2O} (mol/m^3/s)	1.7×10^4
	E_{N_2O} (kJ/mol)	42

For reactions RS.1–RS.4, see Refs. 28 and 39.

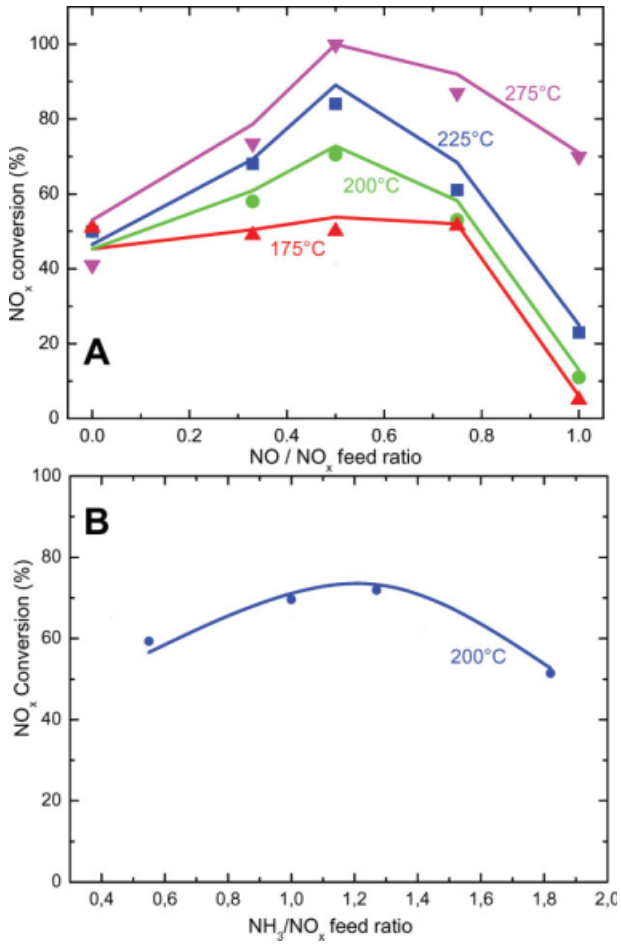

Figure 9. Steady state NO_x conversion at different temperatures versus NO/NO_x feed ratio (A) and at 200°C versus NH_3/NO_x feed ratio (B).

Symbols: measured NO_x conversions. Lines: kinetic fit. [Color figure can be viewed in the online issue, which is available at www.interscience.wiley.com.]

of one of the reactants, clearly shows that the Fast SCR activity is enhanced by increasing the NO_x feed content, whereas it is inhibited by a growing NH_3 feed content. However, such effects were limited to a maximum 10% variation in NO_x conversion under the investigated conditions.

Kinetic fit

The whole set of 42 transient runs performed over the powdered SCR catalyst varying the NO/NO_2 feed ratio, the temperature and the NO_x and ammonia feed concentrations (data in Figures 1–8) was analyzed by global multiresponse nonlinear regression using the dynamic one-dimensional isothermal heterogeneous plug-flow model of the test micro reactor[19] given by Eqs. 25–32.

The estimates of the 12 rate parameters for NH_3 adsorption, desorption and oxidation, and for the Standard SCR reaction, that is, reactions RS.1–RS.4 in Table 1, were taken from the study published in Ref. 28, with no adjustments.

In view of the number of additional fitting parameters required to account for the comprehensive NO/NO_2-NH_3 kinetic scheme, and to minimize correlations, a sequential fitting strategy was followed. Thus, we first estimated the rate parameters associated with formation, adsorption and desorption of nitrates, (r_{amm}, r_{adnit}, r_{desnit}), by regression analysis of runs with feeds containing NO_2 + NH_3 only. In a subsequent stage, the estimate of the rate parameter of the Fast SCR rate expression (D) was secured by regression of runs involving NO + NO_2 + NH_3 at temperatures below 250°C, where the NO_2 SCR reaction was not active. Finally, the rate parameters for Eqs. 23 and 24, that is, the NO_2 SCR (RS.9) and the formation of N_2O (RS.10), were estimated from the high-temperature TRM runs including NO_2 in the feed.

The orders of magnitude of the optimal estimates of the 8 additional kinetic parameters, associated with reactions RS.5–RS-10 in Table 1, are listed in Table 2.

As a result of the regression procedure, the average absolute fitting error was less than 20 ppm for each one of the five responses, which is comparable with the experimental error. The highest absolute value of the extradiagonal terms in the correlation matrix was 0.889, associated with the correlation between k^o_{des} and E^o_{des}.

The goodness of fit can be evaluated by inspection of Figures 1–8, where the solid lines represent model predictions. In all cases, a good agreement is apparent between experimental (symbols) and calculated (solid lines) traces both at steady state and during concentration step changes and transients. This eventually confirms the adequacy of the model in predicting the reactivity of the complete NH_3-NO/NO_2 SCR reacting system over a very wide range of operating conditions, which are close to those of real applications. This clearly appears form Figure 9, which compares the steady state experimental results in terms of NO_x conversions versus both the NO/NO_x (A) and NH_3/NO_x (B) feed ratios with the corresponding model fits.

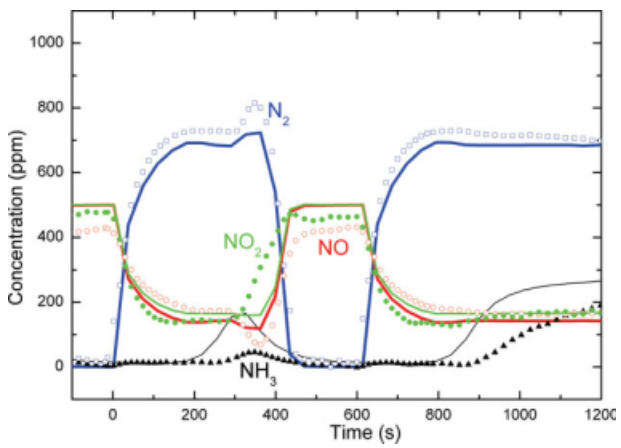

Figure 10. Transient SCR microreactor experiments with subsequent step feed of NH_3 (0, 1000, 0 ppm) in NO (500 ppm) + NO_2 (500 ppm) + O_2 (2% *v/v*) and H_2O (1% *v/v*) + He at 200°C.

Symbols: measured outlet concentrations of NH_3, NO, and N_2 at reactor outlet. Lines: kinetic fit. [Color figure can be viewed in the online issue, which is available at www.interscience.wiley.com.]

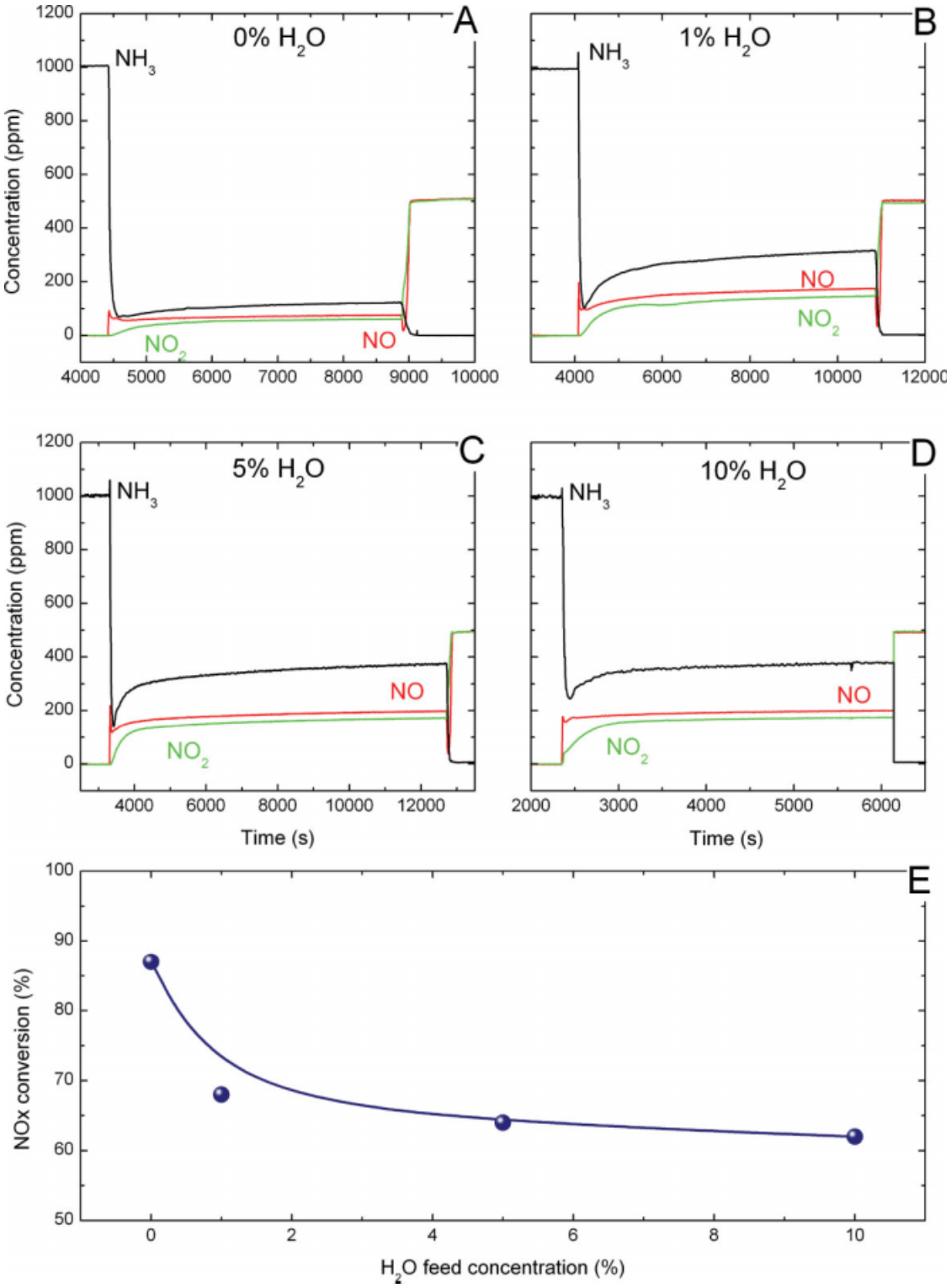

Figure 11. Transient SCR microreactor experiments with step feed of NO (500 ppm) + NO_2 (500 ppm) in NH_3 (550 ppm) + O_2 (2% *v/v*) and H_2O + He at 200°C.

A: H_2O = 0% *v/v*, B: H_2O = 1% *v/v*, C: H_2O = 5% *v/v*, D: H_2O = 10% *v/v*, E: Effect of water on NO_x conversion. [Color figure can be viewed in the online issue, which is available at www.interscience.wiley.com.]

Also, it is worth emphasizing that the model captured satisfactorily the complex transient behaviors observed in the low-temperature runs at the reactants step changes (Figure 10). Even if goodness of fit cannot be taken as a conclusive proof in favor of a proposed kinetic mechanism, this further supports the hypotheses of the unified

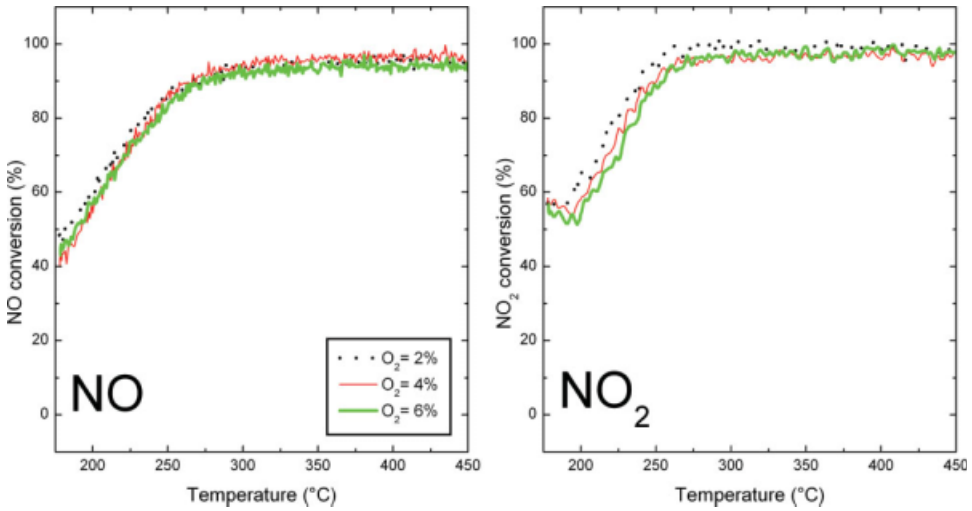

Figure 12. Effect of oxygen feed concentration on steady state NO_x conversions during Fast SCR runs (1000 ppm NH_3 + 500 ppm NO + 500 ppm NO_2 + 1% H_2O in He).

[Color figure can be viewed in the online issue, which is available at www.interscience.wiley.com.]

redox mechanistic scheme on which the present model has been grounded.

Kinetic effects of oxygen and water

We now proceed to further verify the consistency of the mechanistic kinetic model derived in the previous paragraphs with other experimental features.

In fact, additional experiments were performed to study the effects of some operating conditions on the Fast SCR reactivity, namely water and oxygen contents in the feed stream. All the experiments were performed with an equimolar feed concentration of NO and NO_2, that is with a NO/NO_2 feed ratio $R = 1$, and overall NO_x and ammonia concentrations of 1000 ppm.

The effect of water feed concentration in the range 0–10% *v/v* on the Fast SCR reactivity was studied at 200°C by means of TRM runs. Figure 11A/D compares four different experiments carried out with 0, 1, 5, and 10% *v/v* of water in the feed, whereas plot E summarizes the NO_x steady state conversion as a function of water feed content.

A dramatic drop was observed when changing the inlet H_2O content from 0 to 1% *v/v*: for higher H_2O concentrations, the NO_x conversion seemed to stabilize. This means that the presence of water inhibits the Fast SCR reaction, possibly due to competitive adsorption with ammonia. However, water feed contents higher than 1% do not markedly affect the activity of such a reaction, similar to what observed for the Standard SCR reaction.[19]

The effect of oxygen was studied by means of TPR runs with 2%, 4%, and 6% O_2 *v/v* in the feed (Figure 12). In each case 1000 ppm of NH_3, 500 ppm of NO, 500 ppm of NO_2, and 1% of water in He were fed to the microreactor at 175°C. Then a *T*-ramp at 10°C/min was run. Figure 12 shows the NO and NO_2 conversions as a function of catalyst temperature. In all cases at 175°C, a conversion of about 50% was observed independently from the oxygen content in the feed mixture. During the *T*-ramp, the conversions increased; however, the traces remained more or less overlapped. This means that, at variance with what observed for the Standard SCR reaction,[19,28] there was no significant effect of oxygen on the Fast SCR activity over the whole investigated *T*-range.

Both the effects of water and oxygen are consistent with the proposed kinetic model of the Fast SCR reaction, for which the rate is essentially independent of water concentration as indeed observed for water content above 1% *v/v*, whereas oxygen dependence is not apparent because nitrates species can oxidize the catalyst redox sites much more effectively.

Conclusions

We have derived an original, dual-site Mars–van Krevelen kinetic model of both the Standard and the Fast SCR reactions over vanadium based catalysts, which is consistent with a redox catalytic mechanism proposed in the literature and fully accounts for stoichiometry, selectivity and kinetics of the global NH_3-NO/NO_2 SCR process. The present model has the merit to unify Standard and Fast NH_3-SCR kinetics according to a single redox scheme: in the absence of NO_2, it formally reduces to the rate law derived in the past for the Standard SCR reaction only.

Intrinsic rate parameters have been estimated by global nonlinear regression of 42 transient runs performed varying the temperature, the NO/NO_2 feed ratio and the NO_x and ammonia feed concentrations in the absence of diffusional limitations. The model was able to reproduce successfully not only the steady state behavior of the different reacting systems, but also the detailed and complex transient features observed during the dynamic runs. It is currently applied to the development of industrial SCR technologies for vehicles.

Notation

C_i = gas-phase concentration of species i (mol/m^3_{gas})
D_{eff} = effective intraporous diffusivity (m^2/s)
D_K = Knudsen intraporous diffusivity (m^2/s)

D_m = molecular diffusivity (m^2/s)
$E^o_{NH_3}$ = activation energy for ammonia desorption at zero-coverage (kJ/mol)
E_j = activation energy of reaction j (kJ/mol)
G = mass velocity ($kg/m^2/s$)
k^o_j = pre-exponential factors of reaction j
k_j = rate constant of reaction j
k_g = gas-solid mass transfer coefficient (m/s)
k_{1st} = pseudo first-order rate constant for ammonia reaction (1/s)
K_i = adsorption constant for species i (m^3/mol)
p_i = partial pressure of species i (bar)
r_p = average radius of catalyst particle (m)
R = ideal gas constant (J/mol/K)
Re = Reynolds number
r_j = rate of reaction j ($mol/m^3/s$)
Sc = Schmidt number
Sh = Sherwood number
T = temperature (K)
t = time (s)
v = gas linear velocity (m/s)
z = reactor axial coordinate (m)

Greek letters

α = parameter for NH_3 surface coverage dependence in Eq. 10
β = O_2 reaction order in NH_3 oxidation rate law, Eq. 11
ε = void fraction of catalyst bed
ε_p = void fraction of catalyst particle
μ = gas viscosity (kg/m/s)
ρ = gas density (kg/m^3)
σ_i = surface coverage of species i on S_1 sites
τ = catalyst tortuosity factor
θ_i = surface coverage of species i on S_2 sites
Φ^2 = Weisz–Prater modulus
Ω = adsorption capacity of S_2 sites (mol/m^3_{cat})

Literature Cited

1. Johnson T. Diesel engine emissions and their control: an overview. *Platinum Metals Rev*. 2008;52:23–37.
2. Rahkamaa-Tolonen K, Maunula T, Lomma M, Huuhtanen M, Keiski R. The effect of NO_2 on the activity of fresh and aged zeolite catalysts in the NH_3-SCR reaction. *Catal Today*. 2005;100:217–222.
3. Kröcher O, Devadas M, Elsener M, Wokaun A, Söger N, Pfeifer M, Demel Y, Mussmann L. Investigation of the selective catalytic reduction of NO by NH_3 on Fe-ZSM5 monolith catalysts. *Appl Catal B: Environ*. 2006;66:208–216.
4. Wallin M, Karlsson CJ, Skoglundh M, Palmqvist A. Selective catalytic reduction of NO_x with NH_3 over zeolite H-ZSM-5: influence of transient ammonia supply. *J Catal*. 2003;218:354–364.
5. Li M, Yeom Y, Weitz E, Sachtler WMH. Possible reasons for the superior performance of zeolite-based catalysts in the reduction of nitrogen oxides. *J Catal*. 2005;235:201–208.
6. Yeom Y, Henao J, Li MJ, Sachtler WMH, Weitz E. The role of NO in themechanism of NO_x reduction with ammonia over a BaNa-Y catalyst. *J Catal*. 2005;231:181–193.
7. Li G, Jones CA, Grassian VH, Larsen SC. Selective catalytic reduction of NO_2 with urea in nanocrystalline NaY zeolite. *J Catal*. 2004; 234:401–413.
8. Santhosh Kumar M, Schwidder M, Grünert W, Bentrup U, Brückner A. Selective reduction of NO with Fe-ZSM-5 catalysts of low Fe content. II. Assessing the function of different Fe sites by spectroscopic in situ studies. *J Catal*. 2006;239:173–186.
9. Devadas M, Kröcher O, Elsener M, Wokaun A, Söger N, Pfeifer M, Demel Y, Mussmann L. Influence of NO_2 on the selective catalytic reduction of NO with ammonia over Fe-ZSM5. *Appl Catal B: Environ*. 2006;67:187–196.
10. Devadas M, Kröcher O, Elsener M, Wokaun A, Mitrikas G, Söger N, Pfeifer M, Demel Y, Mussmann L. Characterization and catalytic investigation of Fe-ZSM5 for urea-SCR. *Catal Today*. 2007;119:137–144.
11. Sjövall H, Olsson L, Fridell E., Blint RJ. Selective catalytic reduction of NO_x with NH_3 over Cu-ZSM-5: the effect of changing the gas composition. *Appl Catal B: Environ*. 2006;64:180–188.
12. Grossale A, Nova I, Tronconi E. Study of a Fe-zeolite-based system as NH3-SCR catalyst for Diesel exhaust aftertreatment. *Catal Today*. 2007;136:18–27.
13. Grossale A, Nova I, Tronconi E, Chatterjee D, Weibel M. The chemistry of the NO/NO_2-NH_3 "fast" SCR reaction over Fe-ZSM5 investigated by transient reaction analysis. *J Catal*. 2008;256:312–322.
14. Heck RM, Farrauto RJ, Gulati ST. *Catalytic Air Pollution Control*, 2nd ed. New York: John Wiley, 2002.
15. Forzatti P, Lietti L, Tronconi E. *Nitrogen oxides removal—industrial*. In: Horvath IT, editor. *Encyclopedia of Catalysis*, 1st Ed. New York: John Wiley, 2002; and references therein.
16. Koebel M, Elsener M, Kleemann M. Urea-SCR: a promising technique to reduce NO_x emissions from automotive Diesel engines. *Catal Today*. 2000;59:335–345.
17. Koebel M, Elsener M, Madia G. Reaction pathways in the selective catalytic reduction process with NO and NO_2 at low temperatures. *Ind Eng Chem Res*. 2001;40:52–59.
18. Madia G, Koebel M, Elsener M, Wokaun A. The effect of an oxidation precatalyst on the NO_x reduction by ammonia SCR. *Ind Eng Chem Res*. 2002;41:3512–3517.
19. Ciardelli C, Nova I, Tronconi E, Konrad B, Chatterjee D, Ecke K, Weibel M. SCR-DeNO_x for Diesel engine exhaust aftertreatment: unsteady-state kinetic study and monolith reactor modelling. *Chem Eng Sci*. 2004;59:5301–5309.
20. Tronconi E, Nova I, Ciardelli C, Chatterjee D, Bandl-Konrad B, Burkhardt T. Modelling of an SCR catalytic converter for Diesel exhaust aftertreatment: dynamic effects at low temperature. *Catal Today*. 2005;105:529–536.
21. Ciardelli C, Nova I, Tronconi E, Bandl-Konrad B, Chatterjee D, Weibel M, Krutzsch B. Reactivity of NO/NO_2-NH_3 SCR system for Diesel exhaust aftertreatment: identification of the reaction network as a function of temperature and NO_2 feed content. *Appl Catal B: Environ*. 2007;70:80–90.
22. Ciardelli C, Nova I, Tronconi E, Chatterjee D, Bandl-Konrad B. A "Nitrate Route" for the low temperature "Fast SCR" reaction over a V_2O_5-WO_3/TiO_2 commercial catalyst. *Chem Commun*. 2004;23:2718–2719.
23. Nova I, Ciardelli C, Tronconi E, Chatterjee D, Bandl-Konrad B. NH_3-NO/NO_2 chemistry over V-based catalysts and its role in the mechanism of the Fast SCR reaction. *Catal Today*. 2006;114:3–12.
24. Nova I, Ciardelli C, Tronconi E, Chatterjee D, Weibel M. NH_3-NO/NO_2 SCR for Diesel exhausts aftertreatment: mechanism and modelling of a catalytic converter. *Top Catal*. 2007;42:43–46.
25. Tronconi E, Nova I, Ciardelli C, Chatterjee D, Weibel M. Redox features in the catalytic mechanism of the "standard" and "fast" NH_3-SCR of NO_x over a V-based catalyst investigated by dynamic methods. *J Catal*. 2007;245:1–10.
26. Despres J, Koebel M, Kröcker O, Elsener M, Wokaun A. Storage of NO_2 on BaO/TiO_2 and the influence of NO. *Appl Catal B: Environ*. 2003;43:389–395.
27. Apostolescu N, Schroder T, Kureti S. Study on the mechanism of the reaction of NO_2 with aluminium oxide. *Appl Catal B: Environ*. 2004;51:43–50.
28. Nova I, Ciardelli C, Tronconi E, Chatterjee D, Bandl-Konrad B. NH_3-SCR of NO over a V-based catalyst: low-T redox kinetics with NH_3 inhibition. *AIChE J*. 2006;52:3222–3233.
29. Ciardelli C, Nova I, Tronconi E, Ascherfeld M, Fabinski W. Combined use of a mass-spectrometer and a UV analyzer in the dynamic study of NH_3-SCR for Diesel exhaust aftertreatment. *Top Catal*. 2007;42:161–164.
30. Mears DE. Tests for transport limitations in experimental catalytic reactors. *Ind Eng Chem Process Des Develop*. 1971;10:541–547.
31. Topsøe NY, Topsøe H, Dumesic JA. Vanadia/Titania catalysts for Selective Catalytic Reduction (SCR) of nitric oxide by ammonia I. *J Catal*. 1995;151:226–240.
32. Topsøe NY, Dumesic JA, Topsøe H. Vanadia/Titania catalysts for selective catalytic reduction (SCR) of nitric oxide by ammonia II. *J Catal*. 1995;151:241–252.
33. Dumesic JA, Topsøe NY, Topsøe H, Chen Y, Slabiak T. Kinetics of selective catalytic reduction of nitric oxide by ammonia over Vanadia/Titania. *J Catal*. 1996;163:409–417.
34. Wachs IE, Deo G, Weckhuysen BM, Andreini A, Vuurman MA, de Boer M, Amiridis MD. Selective catalytic reduction of NO with NH_3 over supported Vanadia catalysts. *J Catal*. 1996;161:211–221.
35. Willi R, Roduit B, Koeppel RA, Wokaun A, Baiker A. Selective catalytic reduction of NO by NH_3 over Vanadia-based commercial

catalyst: parametric sensitivity and kinetic modelling. *Chem Eng Sci*. 1996;51:2897–2902.
36. Busca G, Lietti L, Ramis G, Berti F. Chemical and mechanistic aspects of the selective catalytic reduction of NO_x by ammonia over oxide catalysts: a review. *Appl Catal B: Environ*. 1998;18:1–36.
37. Chatterjee D, Burkhardt T, Weibel M, Braun T, Tronconi E, Nova I, Ciardelli C. Numerical Simulation of $NO/NO_2/NH_3$ Reactions on SCR-Catalytic Converters: Model Development and Applications. SAE Technical Paper 2006-01-0468.
38. Lietti L, Nova I, Camurri S, Tronconi E, Forzatti P. Dynamics of the SCR-DeNO_x reaction by the transient-response method. *AIChE J*. 1997;43:2559–2570.
39. Chatterjee D, Burkhardt T, Bandl-Konrad B, Braun T, Tronconi E, Nova I, Ciardelli C. Numerical Simulation of Ammonia SCR-Catalytic Converters: Model Development and Application. SAE technical 2005-01-965.
40. Donati G, Buzzi-Ferraris G. Powerful method for Hougen-Watson model parameter estimation with integral conversion data. *Chem Eng Sci*. 1974;29:1504–1509.
41. Villa PL, Forzatti P, Buzzi-Ferraris G, Garone G, Pasquon I. Synthesis of alcohols from carbon monoxide and hydrogen. I. Kinetics of the low-pressure methanol synthesis. *Ind Eng Chem Prod Res Dev*. 1985;24:12–19.
42. Dwivedi PN, Upadhyay SN. Particle-fluid mass transfer in fixed and fluidized beds. *Ind Eng Chem Prod Res Dev*. 1977;16:157–165.

Appendix

Estimate of mass transport limitations in microreactor experiments

The extent of external and intraphase mass transfer limitations in the kinetic runs performed over the powdered V-based SCR catalyst was evaluated according to diagnostic literature criteria, as reported in the following.

Being the process of ammonia adsorption preliminary to the occurrence of all the reactions herein considered and listed in Table 1, its rate must be higher than (or at most equal to) that of any other consecutive reaction, such as the Fast SCR reaction between adsorbed NH_3 and NO and NO_2. Consequently, we focus on verifying the absence of mass transport limitations for NH_3 adsorption. We examine here a run at 425°C with $NO_2/NO_x = 1/2$, corresponding to the highest observed activity, with a NH_3 conversion of about 96%.

The absence of interphase (gas-solid) mass transfer limitations was checked by the following criterion[30]

$$\frac{k_{1st} d_p}{6 \cdot k_g} < 0.05$$

where:

k_{1st} (1/s) = pseudo 1st-order rate constant for NH_3 conversion,

d_p (m) = average diameter of the 140-200 mesh sieved catalyst powder loaded in the reactor = 90×10^{-6} m,

k_g (m/s) = gas-solid mass transfer coefficient.

From the NH_3 conversion data, and from a catalyst contact time of 0.017 s, we estimate $k_{1st} = 190$ 1/s. For estimation of k_g, we apply the following correlation, recommended for the range $0.01 < Re < 15{,}000$[42]:

$$\varepsilon j_m = \frac{0.765}{Re^{0.82}} + \frac{0.365}{Re^{0.386}}$$

where:

ε = catalyst bed porosity,

$$j_m = \frac{Sh}{ReSc^{1/3}},$$

$$Sh = \frac{k_g d_p}{D_m}, \quad Re = \frac{G d_p}{\mu}, \quad Sc = \frac{\mu}{\rho D_m},$$

with D_m being the molecular diffusivity of NH_3 in the He-rich gas mixture ($\approx 3 \times 10^{-4}$ m^2/s), and with other obvious symbols reported in the Notation.

For the assumed conditions, Re = 0.09, Sc = 1.4, and Sh = 2.0, which yields $k_g = 6.5$ $m^3/m^2/s$, and

$$\frac{k_{1st} \cdot d_p}{6 \cdot k_g} = 4.6 \times 10^{-4} < 0.05$$

The occurrence of external mass transfer limitations is thus ruled out.

The extent of intraparticle concentration gradients was verified by the Weisz–Prater criterion[30]:

$$\Phi^2 = \left(\frac{d_p}{6}\right)^2 \frac{k_{1st}}{D_{eff}} < 0.08$$

where:

Φ^2 = Weisz–Prater modulus,

D_{eff} = ammonia effective intraporous diffusivity, herein evaluated as:

$$D_{eff} = \frac{\varepsilon_p}{\tau}\left(\frac{1}{D_m} + \frac{1}{D_K}\right)^{-1}$$

According to measurements of the catalyst morphology, the catalyst porosity was 0.62 m^3/m^3, whereas the bimodal pore size distribution was associated with average pore radii of 160 Å (mesopores) and of about 1000 Å (macropores). Adopting a conservative approach, where we consider only the mesopores, the Knudsen diffusivity is $D_K = 1.0 \times 10^{-5}$ m^2/s and, on assuming a tortuosity factor $\tau = 4$, we get $D_{eff} = 1.5 \times 10^{-6}$ m^2/s, so that

$$\Phi^2 = 0.028 < 0.08$$

Thus, also intraphase mass transfer limitations can be ruled out.

Manuscript received July 28, 2008, and revision received Oct. 8, 2008.